The use of assay data as a foundation for a geometallurgical model – the case of the Thaba Chromite Mine, South Africa

Bachmann, K.; Menzel, P.; Tolosana-Delgado, R.; Schmidt, C.; Hill, M.; Gutzmer, J.;

Originally published:

February 2019

Journal of Geochemical Exploration 201(2019), 99-112

DOI: https://doi.org/10.1016/j.gexplo.2019.01.008

Perma-Link to Publication Repository of HZDR:

https://www.hzdr.de/publications/Publ-27582

The use of assay data as a foundation for a geometallurgical model—The case of the Thaba Chromite Mine, South Africa

Kai Bachmann, Peter Menzel, Raimon Tolosana-Delgado, Christopher Schmidt, Moritz Hill, Jens Gutzmer

PII: S0375-6742(18)30364-9
DOI: https://doi.org/10.1016/j.gexplo.2019.01.008
Reference: GEXPLO 6257

To appear in: *Journal of Geochemical Exploration*

Received date: 14 June 2018
Revised date: 7 December 2018
Accepted date: 23 January 2019

Please cite this article as: K. Bachmann, P. Menzel, R. Tolosana-Delgado, et al., The use of assay data as a foundation for a geometallurgical model—The case of the Thaba Chromite Mine, South Africa, Journal of Geochemical Exploration, https://doi.org/10.1016/j.gexplo.2019.01.008

The use of assay data as a foundation for a geometallurgical model – the case of the Thaba Chromite Mine, South Africa

Kai Bachmann[1,2]*, Peter Menzel[3], Raimon Tolosana-Delgado[1], Christopher Schmidt[4], Moritz Hill[4], Jens Gutzmer[1]

[1]Helmholtz-Zentrum Dresden-Rossendorf, Helmholtz Institute Freiberg for Resource Technology, Chemnitzer Str. 40, D-09599 Freiberg/Sachsen, Germany

[2]Department of Mineralogy, TU Bergakademie Freiberg, Brennhausgasse 14, D-09596 Freiberg/Sachsen, Germany

[3]Department of Geophysics and Geoinformatics, TU Bergakademie Freiberg, Gustav-Zeuner-Str. 12, D-09596 Freiberg/Sachsen, Germany

[4]Cronimet Mining Group, Building C Willow Wood Office Park, Cnr 3rd & Cedar Roads, Broadacres 2021, Johannesburg, South Africa

*Tel: +49 351 260 4426

k.bachmann@hzdr.de

Working Title: Defining Geochemical Domains, western Bushveld

Introduction

The main source of mineable chromium occurs naturally as chromite, a chromium spinel with the chemical formula ($[Mg, Fe^{2+}][Cr, Al, Fe^{3+}]_2O_4$). Around 90 % of the mined chromite is processed in the metallurgical industry for the production of stainless steel, alloyed steel and nonferrous alloys (USGS 2018). South Africa accounts for roughly 45 % of the global annual chromite ore production and for 40 % of the current world's chromite reserves (USGS 2018). These reserves are associated with the Bushveld Complex, the largest layered mafic-ultramafic intrusion worldwide, which was emplaced into the supracrustal rocks of the Transvaal Supergroup approximately 2,055 Ma ago (Zeh et al. 2015). The chromite is hosted by ultramafic and mafic rocks of the Rustenburg Layered Suite (RLS) which is divided into the Marginal, Lower, Critical, Main and Upper Zones (Maier et al. 2013, Figure 1A).

Besides vast resources of chromite, the Critical Zone of the RLS represents the largest global resource of platinum-group elements (PGE) as well as significant resources of Ni and Cu (e.g., von Gruenewaldt 1977; Maier et al. 2013). A significant portion of the geological PGE resources is hosted together with chromite in a series of 14 major chromitite seams. According to their stratigraphic position in the Critical Zone the chromitite seams have been subdivided into the Lower, Middle and Upper Groups (LG (7 seams), MG (4 seams), UG (2 seams), Figure 1B). The major chromitite seams have, in general, a decreasing content in chromium, ranging from >46% Cr_2O_3 in the lower LG seams, to <42% Cr_2O_3 in the UG seams. This trend is accompanied by a decrease of their Cr/Fe ratio from >1.8 to <1.3 (e.g., Fourie 1959; Viljoen 2016) and an increase of the Σ[PGE+Au] concentrations ranging from <1 ppm in seams LG -1 to LG-4, up to 10 ppm in the UG-2 chromitite (Von Gruenewaldt et al. 1986; Scoon and Teigler 1994). Therefore, the LGs

and MGs are mined for chromite as a main (and currently only) product while the UG2 chromitite is currently mined for PGE as the main product and chromite a by-product (Viljoen 2016). Successful attempts were recently initiated to reprocess chromite dumps originating from the LG-6 and MG-1/2 chromitites to produce saleable concentrates of both chromite and PGE (Oberthuer et al. 2016). However, in general, chromitites of the LG and MG seams are currently still regarded as sub-economic for PGE production. This is despite the fact that by the extraction and beneficiation of chromite all costs for infrastructure as well as expenses for mining, transport and comminution are already covered. Furthermore, the tailings remaining from chromite beneficiation are markedly enriched in PGE, hosted either in discrete platinum group minerals (PGM) or in solid solution with base metal sulphides (BMS). The above is also the case for the Thaba Mine (operated by Cronimet Chrome Mining SA (Pty) Ltd, a subsidiary of the Cronimet Mining Group), located in the north-western sector of the Bushveld Complex, approximately 25 km southwest of Thabazimbi and 85 kilometres northwest of Rustenburg. Beside the LG-6 and LG-6A chromitite, open-cast mining is undertaken on the MG-1 to MG-4A for chromite as the primary economic mineral. Mining started in 2011 and the life of mine is estimated at 26 years.

The bulk of the LG and MG chromitites extracted in the Bushveld Complex has an orthomagmatic mineral assemblage dominated by chromite (>50 wt% to 95 wt%) and associated gangue silicates, predominantly orthopyroxene and plagioclase (Kinnaird et al. 2002). Base metal sulphides (BMS) and platinum group minerals (PGM) occur only in trace amounts. This orthomagmatic assemblage has been noted to be affected by surficial weathering (down to 50 m; Wagner 1929; Junge et al. 2015) and hydrothermal alteration (e.g. Penberthy and Merkle

1999; Voordouw et al. 2010). Published knowledge on the effect of supergene and hydrothermal alteration on the mineralogy of the chromitites in the Bushveld Complex is, however, scant (e.g. Hey 1999; Becker et al. 2014). Becker et al. (2014) report an enrichment of alteration silicates (amphibole, chlorite, serpentine, talc) and Fe-oxides/hydroxides, as well as depletion in BMS as a result of weathering. This is similar to comparable altered and oxidized PGE ores elsewhere (Oberthür et al. 2003).

This change in gangue mineralogy will have significant impact on the chromite beneficiation process, for both the grinding and the beneficiation circuits. The effectiveness of the grinding circuit is highly sensitive to variations in feed composition. A shift in mineralogy towards alteration silicate-rich chromitite compositions will result in a higher amount of fines, which will reduce the performance of the subsequent unit operations (Murthy et al. 2011 and references therein). Equally important will be the effect of alteration on density separation techniques, such as spirals; an increase in fine particle sizes (<100 µm) will negatively impact the recovery during gravity separation – a significant amount of chromite will be lost to the tailings (Gence 1999). Murthy et al. (2011) reported that up to 25 % of the mineral value originally contained in the chromite ore is lost as slimes during beneficiation.

On the other hand, oxidized ores display a loss of Pd relative to Pt due to the increased mobility of Pd in supergene environments (e.g. Oppermann et al. 2018). Remobilization of Pd in oxidized PGM ores is also believed to reduce flotation efficiency by changing the Pt:Pd ratio, which is the key metric used in the processing of PGE ores of the Bushveld Complex (Becker et al. 2014). In supergene ores, PGE occur (i) as relict primary PGM, (ii) in solid solution with relict BMS, (iii) as secondary PGE alloys, (iv) as PGM oxides/hydroxides and (v) as PGE hosted by secondary

oxides/hydroxides (e.g. Fe, Mn) or silicates (e.g. smectite, chlorite) (e.g., Evans et al. 1994; Oberthür et al. 2013; 2003). While the beneficiation of PGE from pristine sulphide ores achieves platinum recoveries above 80 %, processing of oxidized ores by conventional flotation techniques typically results in very poor PGE recoveries below 50 %; this is regarded as uneconomic (e.g., Evans 2002; Locmelis et al. 2010; Becker et al. 2014; Sefako et al. 2017). To improve PGE recoveries, alternative processing routes have been tested with variable success – as recently summarized by Sefako et al. (2017; and references therein).

The scope of this study is to investigate the bulk geochemistry of a large number of drill cores of four chromitite seams of the Thaba mine, to discuss the variability within and between the distinct seams and to separate the mine lease area into distinct geochemical clusters. These clusters are then related to the geological architecture in the mine lease area. The results are then combined with knowledge concerning the quantitative mineralogical composition of selected samples. This leads to the definition of domains that can be clearly distinguished based on their mineralogical, geochemical and geological characteristics. It is expected that these can also be used as a solid foundation of a geometallurgical model for the deposit.

Geology and geochemistry of the Thaba Mine

The delineation of mineral resources at Thaba Mine was carried out according to the guidelines of the South African Mineral Resource Committee (SAMREC, www.samcode.co.za). Exploration on the lease area took place in three drilling campaign and one trenching program from June 2008 until March 2011. Chromitite seams were sampled and chemically analysed for major element oxides (Cr_2O_3, FeO, SiO_2, MgO, Al_2O_3, CaO) and phosphorous concentrations in order to

estimate the mineral resource. Analyses were carried out batch-wise by two certified laboratories in South Africa (METCHEM until mid-2009; Setpoint starting mid-2009).

At Thaba mine, the RLS was found to dip to the southeast at angles between 15 to 27 degrees. Of the four targeted seams used in this study the LG-6 is the most valuable for chromite production. It averages 0.85 m in thickness (ranging from 0.34 m to 1.37 m), and generally comprises a single seam with minor thin pyroxenite partings. The Cr_2O_3 content averages 43.1 wt% and the Cr:Fe ratio is 1.58. The LG-6A occurs in close vicinity to the LG-6 and has an average width of 0.23 m, containing 41.2 wt% Cr_2O_3 with a Cr:Fe ratio of 1.48. The MG-1 seam has an average of 0.59 m in thickness and is best developed in the north-eastern sections of the lease area. Cr_2O_3 contents average at 36.8 wt% and a Cr:Fe ratio around 1.41 makes the MG-1 a potential target in that area, in addition to, or instead of the LG6. Only four MG1 intersections were drilled in the southwest of the mine lease area. The MG-2 is only slightly thinner than the MG1 (Ø: 0.53 m) but in 34 of the 117 intersections it is split by a barren pyroxenite parting of up to a meter thickness. With an average content of 35.5 wt% Cr_2O_3 and low Cr:Fe ratios around 1.30 it is a potential target for chromite exploitation in an open-cast scenario only.

The RLS and its chromite seams on the Thaba mine lease area are crosscut by a number of younger lithologies and geological structures. Most prominent is a pipelike, olivine-clinopyroxene pegmatite (iron-rich ultramafic pegmatite; IRUP) occurs (Scoon and Mitchell 1994). It has a surface diameter averaging 1.5 km and is situated entirely within a graben with a down throw of over 500 m (Viljoen and Scoon 1985). Furthermore, there is a series of NW-SE striking faults, some of which have been intruded by thin mafic dykes. All of these lithologies are

overlain by a thin veneer of (autochthonous) soil associated with chemical weathering to a depth of about 50 m below the present-day land surface.

Bachmann et al. (2018) described in detail the least altered mineral assemblages of the LG-6 and LG-6A chromitite seams at Thaba mine; these are dominated by chromite and minor ortho- and clinopyroxenes, feldspar, micas, olivine and trace amount of quartz. Alteration minerals identified include carbonates (calcite/dolomite) and silicates such as amphiboles, chlorite, serpentine and talc.

The wide variety of accessory minerals identified by Bachmann et al. (2018) includes base metal sulphides, platinum group minerals, apatite, monazite, zircon, as well as barite, rutile and titanite. Bachmann et al. (2018) concluded that no truly unaltered orthomagmatic mineral assemblage is preserved at the Thaba Mine but that alteration assemblages are similar in both of the two studied chromitite seams. Importantly, lateral variation between different drill cores dominates over vertical variation within seam, as well as between the LG-6 and LG-6A seams.

Data and Methodology

This section is divided into two subsections. In the first subsection, available data and the methodology used to generate the geological model are documented. The treatment of the geochemical data set is explained in a separate subsection.

Geological Model

The geological 3D model is based on 270 of the >400 available drill core logs. All selected boreholes provided a collar location ($\vec{c}$), geo-referenced with a Cartesian coordinate system called Hartebeesthoek94 / Lo27 (reference meridian 27°, east), a depth (D) representing the

total borehole length and survey information that contain dip (dip) and bearing (b) angles in degree at several depth positions in each borehole. No additional coordinate system transformation was applied for modeling the 3D geometry and plotting the data. The collar locations are displayed by black dots in Figure 2A. Additionally, known faults (red lines) in the modelling area and the mine lease area (magenta polygon) are illustrated. Since no dip information was available for the faults, they were treated as vertical. Fourteen different fault blocks (grey polygons in Fig. 2A) were generated. Each borehole was allocated to its corresponding fault block.

The topography information of the mine area, based on the 90 × 90 m SRTM grid of Jarvis et al. (2008), was used for the modelling purposes and corrected by the collar heights (black isolines in Figure 2A & B). Since all measurements were taken from drill core samples, the first modelling needed is the derivation of the three dimensional geometry of all borehole paths. The 3D geometry for each path is calculated based on the collar position $\vec{c} = \{c_x, c_y, c_z\}$ and the survey information. At first, the survey angles at a depth $d, 0 \leq d \leq D$ are transferred into a three dimensional directions vector ($\overrightarrow{v_d}$):

$$\overrightarrow{v_d} = \{\sin(dip_d - 90°)\cos(b_d), \sin(dip_d - 90°)\sin(b_d), \cos(dip_d - 90°)\}.$$

The normalized directions are interpolated at the depth positions for all lithological units given in the borehole logging by using a 2nd-order spline interpolation. All interpolation depth values d' with $0 \leq d' \leq D$ are ordered by increasing d' with $d'_i > d'_{i-1}$ and $d'_0 = 0$. The 3D positions $\vec{P}_{d'_i}$ for all values d'_i are incrementally calculated by:

$$\vec{P}_{d'_i} = \begin{cases} \vec{c} & \text{for } i = 0 \\ \vec{P}_{d'_{i-1}} + \vec{v}_{d'_i}(d'_i - d'_{i-1}) & \text{for } i > 0 \end{cases}.$$

Based on the drill core logs, a set of stratigraphically distinct lithological units was defined including all chromitite seams from LG-1 to UG-1 and their host rock units. All logged lithologies are assigned to one of these stratigraphic units: silicate rocks (dunite, norite, harzburgite, etc.), chromitite (LG-1 to UG-1), overburden (saprolite, soil), structural features (faults, dykes) and altered rocks. Altered rocks comprise all macroscopically visible alteration features (alteration – unspecified such as altered pyroxenite, altered norite, etc.; carbonate; serpentine) and features that are known to induce alteration to their host rocks (IRUP; (replacement) troctolite; Viljoen and Scoon 1985; Reid and Basson 2002; Voordouw et al. 2010).

In the next step, the 3D points for the hanging wall and footwall contacts were extracted for the four target chromitite seams (LG-6, LG-6A, MG-1 and MG-2). A 3D surface for the top and bottom contacts was interpolated for each fault block separately by using the DSI algorithm (Discrete Smooth Interpolation; e.g. Mallet 2002) of the Paradigm® **SKUA-GOCAD™** software. The modelling is performed within each of the fault block polygons to ensure a smooth interpolation. Since most of the incorporated 3D positions are located inside the mine leasing area (magenta polygon, cf. Figure 2), surface parts outside the mine lease area are only based on interpolation. The interpolated surfaces were cut by the topographic surface. Fault blocks containing insufficient data are represented by mean planes lacking information such as strike and dip. Figure 3A displays the resulting depth maps (left) and 3D shapes (right) of LG-6 and MG-1. The modelled 3D surfaces (Figure 3B) are then used as spatial domains for geostatistical interpolations, for visualization and for a spatial relation of the geochemical assays with local geology and structural features.

Geochemical Data

Concentration data for Cr_2O_3, FeO, Al_2O_3, MgO, SiO_2, CaO and P (as a penalty element during ferrochrome production, Goel 1997) were provided by Cronimet SA (Pty). After careful interrogation of the data a data set of 771 assays (LG-6: 339; LG-6A: 242; MG-1: 57; MG-2: 133) consisting of motherholes and/or deflection drill holes was processed further ([dataset] Bachmann et al. 2018). Cronimet received the assay data from two commercial laboratories, Setpoint Laboratories (Johannesburg) and METCHEM Laboratories (Johannesburg), within a time frame of almost four years. In both laboratories, major element analysis was carried out by X-ray fluorescence spectrometry (XRF) on fused glass beads. The involvement of two laboratories – and the fact that batches of samples were submitted over an extended period of time – carries the risk of systematic errors between different sample batches represented in the data base. Other sources of error include 1) sample collection and preparation, 2) daily signal drifts within individual measurement runs, and 3) systematic differences between different analytical methods used. To detect and minimize such errors, Cronimet SA (Pty) has conducted a comprehensive program of quality control and quality assurance (QAQC) for all core samples, similar to what is suggested in literature (e.g., Abzalov 2008 and references therein). Firstly, 23 un-mineralised leuconorite samples were randomly inserted as blanks into the sample batches in order to monitor possible contamination and sample swaps. All leuconorite samples recorded Cr_2O_3 and FeO below the set threshold limit (<1% Cr_2O_3; <10% FeO). Furthermore, a total of 62 quarter core field duplicate samples were taken for the target seams and submitted to the geochemical laboratories with different sample identification numbers to the original as blind duplicates in order to check for sampling and analytical error. The scatter plots for Cr_2O_3 and FeO display in general deviations of less than 10 % for duplicates (Figure 4). Few analyses of MgO and Al_2O_3 exceed this limit. Furthermore, internationally certified standards of South

African chromite ores (SARM8 and SARM9) were randomly inserted to monitor Cr_2O_3 and FeO accuracy at Setpoint Laboratories. An acceptance criterion of ±3σ was used for these standard data. One SARM8 sample returned a Cr_2O_3 grade marginally above 2σ from the mean while FeO tended to be assayed at a lower grade than its certified mean, with one analyses close to the 3σ acceptance criterion. All SARM9 samples returned assays for Cr_2O_3within the acceptable range. The FeO value of this standard tended to be reported at a lower concentration than the certified value but within 3σ of the certified mean.

Working with compositional data

A set of variables form a composition, if their size (or total sum) is irrelevant, or if it is an artefact of the sampling procedure (van den Boogaart and Tolosana-Delgado 2008). Whenever this happens, but the ratios between the components are believed to still inform of the relative concentrations between the components, one is forced to close the data to sum to 100% in order to be able to compare the percentages among samples. Whole rock geochemical (assay) data do most commonly fall in this framework (van den Boogaart and Tolosana-Delgado 2008). When working with closed data, and compositional data in general, one should be aware that *spurious correlation effects* occur (Pearson 1897; Chayes 1960) and standard statistical methods applied to raw or closed compositional data might lead to inconsistent results (e.g., Tolosana-Delgado et al. 2005). To get rid of these effects, the solution chosen here is to work with ratios or log-ratios between components, within the framework of the so called Compositional Data Analysis (Aitchison, 1986).

Testing batch differences and correction of data for further statistical treatment

As this study deals with a multivariable data set, appropriate multivariate statistical techniques such as discriminant analysis, cluster analysis, or principal component analysis (PCA), should be used for data processing, revealing the most relevant trends without external supervision (e.g. Koch 2012; Frenzel et al. 2016). This works well in homogeneous data sets (e.g., Engelbrecht 1985; De Waal and Gauert 1997, Smart et al. 2017), however, in heterogeneous data sets, composed of several batches (e.g. of data from different geochemical laboratories), data quality might not be always sufficient to warrant the homogeneity in population required by further statistical analysis. As described in De Gruijter et al. (2006), various procedures for a consistent sampling of spatial data sets exist, such as simple random sampling or, if the number of batches is known, sampling using an interpenetrating space–time grid.

In the present case, the spatial sampling procedure to create batches for geochemical analysis does not follow the methodology described by De Gruijter et al. (2006); hence, data should be tested for consistency. At Thaba mine, batches were partly created on a regional basis, making it difficult to distinguish between systematic lab-based differences and spatial compositional differences. As an example, Figure 5 shows the batches created for the LG-6. While batch 1 was sent to METCHEM, the others were analysed by Setpoint. As batch 1 and batch 2 comprise only motherholes and deflections, respectively, these are the only batches where a correction of possible analytical uncertainties is conceivable.

To test if a correction of batches is necessary, a linear discriminant analysis (LDA; Fahrmeir and Hammerle 1984) based on a batch-wise classification was performed with the isometric log ratio transform (Egozcue et al, 2003) of the data set for every seam separately through a linear combination. Data analysis was performed within the R software environment (R Core Team

2016) with the additional packages “mclust” (Fraley and Raftery 2002), “MASS” (for function “lda”; Venables and Ripley 2002) and “compositions” (van den Boogaart et al. 2014). LDA maximizes the ratio of between-class to within-class variances in our data set thereby guaranteeing maximal separability. In a batch-wise classification separation should be reduced to a minimum and samples should be rather homogeneous.

As an example, results for the LG-6 are shown in more detail (Figure 6). Linear discriminant 1 (LD 1) led to a clear separation of batch 2 from batch 1, 3 and 4, whereas 80 out of 88 analyses would be reclassified as batch 2 (Figure 6A). The close spatial relationship of motherholes and deflections (between batch 1 and 2) excludes compositional differences based on geological reasons – but may reflect sampling and/or analytical uncertainties. Batch 3 strongly scatters and might be separated from batch 1, 2, and 4 by LD 2. However, only 20 out of 35 analyses would be reclassified as batch 3 implying that no systematic sampling and/or analytical uncertainties are responsible for the separation. Furthermore, LD1 explains almost 80 % of the between-group variance, while LD2 is responsible for another 15 % (scaling of LD1 and LD2 is displayed in Figure 6B).

At this point, we have two choices. We either could discard the full dataset or sacrifice some information to maximize the possible outcomes of the database. We decided to go with the latter and minimized the detected analytical uncertainties by reducing the compositional contrast between batch 1 and batch 2 by matching the compositional means of each suite (i.e. by perturbing each composition $x = [x_1, x_2, \dots, x_D]$ batch 2 by a vector of constants), and reclosing them to sum to 100%,

$$x^* = 100\frac{[x_1k_1, x_2k_2, \dots, x_Dk_D]}{x_1k_1 + x_2k_2 + \cdots + x_Dk_D}$$

where the perturbation factors are computed as the ratios of the compositional means of batch 1

$m_1 = [m_{11}, m_{21}, \dots, m_{D1}]$ to the compositional means of batch 2 $m_2 = [m_{12}, m_{22}, \dots, m_{D2}]$:

$k_i = \frac{m_{i1}}{m_{i2}}$.

In these equations, D represents the number of geochemical components analysed, and each x_i or m_{ij} represent the percentage of element i on a specific sample, respectively on the compositional mean of batch j.

Results of the correction are displayed in Figure 6C. Batches 1 and 2 display the same compositional mean; other properties such as variance, co-dependence between variables, etc. are not changed. The resulting numbers for batch 2 samples cannot be any more interpreted in terms of mass ratios of the elements considered, but they still fully capture the variability and structure displayed by the original data. Only the systematic differences between batches have been removed.

Such batch-wise correction was applied to all target seams, where it appeared to be meaningful and/or necessary. Detailed information about the batches and their correction for all seams can be found in Table 1. In the cases of the LG-6 and LG-6A chromitite seams batch 2 represents the deflections while batch 1 represents the motherholes and was therefore shifted. Batches 2 and 3 of the MG1 chromitite seam represent a similar area of the mine and are strongly spatially

interfering; the same is true for batch 1 and 3 in the MG2 chromitite seam, making a correction meaningful.

Results

The results section is divided in two parts. Firstly, some results concerning the geological model are provided. Secondly, we evaluate the geochemical data set.

Alteration in the Geological Model

As described above, the lithological units modelled separately comprise silicate host rocks, chromitite seams (with special focus on the target seams) and different types of alteration, such as carbonate alteration, serpentinization, etc. To represent and, hence, to interpret the geochemical data in a spatial framework the relationship between alteration markers and certain geochemical clusters is of particular interest. Figure 7 displays all alteration markers detected in the core logging data within each borehole. While Figure 7A shows only troctolite alteration, which is mainly located in the southern part of the deposit, Figure 7B displays all other alteration types. The dominance of carbonate alteration at the northern edge of the deposit is clearly visible as well as significant serpentinization in the central part of the Thaba mine lease area. IRUP bodies seem to be mainly distributed in the northern part of the mine lease area, especially around the Middellaagte IRUP but rarely occur in the south.

Covariance structure of the data sets

A series of boxplots for the different sample populations (Figure 8) provides a first impression of the variability of the data set. The variability of the major element oxide and P concentrations for the four seams LG-6, LG-6A, MG-1 and MG-2 is illustrated. Contrasts between the LGs and

MGs are clearly visible for some elements (e.g., Cr, Si, Ca) but are minimal between the LG-6/LG-6A as well as MG-1/MG-2. Some major element oxide concentrations follow general stratigraphic trends that are well-documented for the chromitite seams of the RLS, including a decrease of Cr_2O_3 that is matched by an increase of SiO_2, Al_2O_3 and CaO. Concentrations of FeO, MgO and P, in contrast, remain rather constant (e.g. Scoon and Teigler 1994).

Principal component analysis (PCA) displayed as compositional biplots (e.g. Aitchison 1990; Eynatten et al. 2016) was performed to inspect the covariance structure of the data set. The data has been centred log ratio (clr) transformed (Aitchison compositions, Aitchison 1990), implying that the centre of the biplot corresponds to the compositional mean of the data set.

The elemental biplot of the corrected data set reveals a grouping of the data depending on the seam (Figure 9A). The first principal component (PC1) reflects 66 % of the total variability and is characterized by strong positive loadings of CaO and SiO_2 and negative loadings of Cr_2O_3, FeO, P, Al_2O_3 and MgO. In general, the chromite control of Cr_2O_3, FeO, and Al_2O_3 concentrations and to a lesser extent also MgO contents becomes obvious. The second principal component (PC2) captures 18 % of the variability and displays positive loadings for CaO, P and FeO and negative loadings for SiO_2 and MgO. PC1 effectively separates chromite-rich rocks from rocks more enriched in silicates and/or carbonates, i.e. the LG from the MG chromitites. PC2 separates slightly more chromite-rich rocks of the LG-6 from the LG-6A and, furthermore, carbonate enriched samples are separated from more silicate-rich rocks. In general, the first two principal components gradually order the different chromitite seams from the LG-6 stratigraphically upwards (red arrow). Nevertheless, the PCA reveals only little variation within the data set with minor exceptions. The elemental biplot in Figure 9B combines PC1 and PC3, which captures

11 % of the variability in the data set. PC3 is characterized by a strong negative loading of P resulting in a systematic variation of the LGs along the y-axis; in contrast, the MG's almost show no systematic trend but a scattering of the data along PC3.

Perturbing the compositional means of LG-6A, MG-1 and MG-2 by the difference of the inverse compositional mean of LG-6 (as was done for correcting the systematic differences between batches) allows for focusing the biplot analysis on features controlled by parameters other than seams, such as depth of the intersection. In the resulting biplot (Figure 9C), PC1 captures 60 %, PC2 21 % and the overall loadings are similar to Figure 9A. Data distribution is twofold: (i) data distribution is rather homogeneous for all depth classes deeper 50 m (with a slight shift to SiO_2-richer compositions), (ii) data of depth class below 50 m is mainly characterized by positive scores on PC1, and either positive or negative scores on PC2 translating to rather high proportions of CaO and/or SiO_2.

Cluster analysis

Cluster analysis was performed separately for LGs and MGs, respectively, using the compositions corrected for batch difference: a cluster of the non-corrected data showed only groups based on the batches, a result of no scientific relevance. Figure 10A displays a distinct separation into four clusters for geochemical data of the LG-6 and LG-6A. While cluster 1 represents samples high in Cr_2O_3 and low in CaO/SiO_2, cluster 2 shows a slight but systematic shift to SiO_2 and CaO enriched compositions. Cluster 3 is dominated by outliers with high CaO and/or SiO_2 contents, while Cr_2O_3 shows, in general, lower concentrations. The "supergene" cluster represents all drill core intersections classified as cluster 2 and are within the first 50 m below surface. Whether the drill core intersections of this cluster were already altered prior to

being exposed to weathering cannot be determined. Additionally, the results display systematic trends which are independent from the considered seam.

Figure 10B shows the results of the corresponding cluster analysis for MG-1 and MG-2. Note that PC3 is shown on the y-axis, displaying similar loadings as PC2 in Figure 10A. On the other hand, PC2 of the MGs corresponds to PC3 of Figure 10B (as well as PC3 of the LG's), showing strong loadings on phosphorous. For comparison, the loadings for the first three PCs (capturing 90 % of total variability) are displayed in Table 2. Hence, due to limited data points, cluster discrimination for the MG chromitites is not as significant as for the LGs but appearing more "noisy". Nevertheless, overall trends are similar to the LGs, representing a shift towards SiO_2/CaO richer compositions from cluster 1 through cluster 2 to the "Supergene" cluster. As shown in Figure 10A, cluster 3 predominantly represents outliers with either high phosphorous or CaO contents. Similar to the LG-6/LG-6A, trends do not distinguish MG-1 from MG-2.
Figure 11A and 11B summarize the results for LGs and MGs, respectively, by displaying the arithmetical means of geochemistry for each cluster. A decrease in Cr_2O_3 concentration from cluster 1 to the "Supergene" cluster is evident in these diagrams. Phosphorous concentrations are not shown but they are constant at ca. 20-30 ppm (corrected) for all clusters within the LGs and the MGs, except cluster 3. Cluster 3 displays mean of ca. 75 ppm and 100 ppm of phosphorous for LGs and MGs, respectively.

Linking geochemistry with mineralogy

The mineralogy of chromitite seams of the LGs and MGs is well known and has been already described in detail (Naldrett et al. 2009, 2012 and references therein) as well as for the Thaba Mine lease area (Bachmann et al. 2018). Cr_2O_3 occurs almost exclusively in chromite ([Mg,

Fe^{2+}][Cr, Al, Fe^{3+}]$_2O_4$). Mineral compositions of chromite show only slight variation, thus the assumption to link increasing Cr_2O_3 contents with increasing chromite concentrations is valid. Considering an magmatic origin of the chromitites (Naldrett et al. 2009, Maier et al. 2013), expected silicate minerals are orthopyroxene (enstatite ($Mg_2Si_2O_6$) – ferrosilite ($Fe_2Si_2O_6$)), minor clinopyroxene (diopside ($MgCaSi_2O_6$) – hedenbergite ($FeCaSi_2O_6$)), olivine ($(Mg,Fe)_2[SiO_4]$), feldspar ($(Ca,Na,K)(Al,Si)_4O_8$; mainly plagioclase) and dark micas with biotitic compositions ($K(Mg,Fe^{2+},Mn^{2+})_3[(OH,F)_2|(Al,Fe^{3+},Ti^{3+})Si_3O_{10}]$). Important minor and trace elements, not shown in the general mineral formula, in these minerals are V, Ti and Mn. According to the expected minerals the chemical assays used in this study include all important elements, with minor exceptions usually accounting for not more than 1-2 wt% in total. Furthermore, iron was only measured as FeO, but in reality, iron is present as both FeO and Fe_2O_3, which again will account for another few wt% in total. It can be concluded that the chemical assays contained in the data base should account for >97 wt%. As shown earlier, there is a significant positive correlation between low totals and mainly SiO_2 and CaO. Hence, there are significant numbers of analyses with totals below 95 wt%. These can be explained by alteration of certain mineral assemblages. Bachmann et al. (2018) showed that significant amounts of alteration silicates, such as chlorite ($(Fe,Mg,Al,Zn)_6(Si,Al)_4O_{10}(OH)_8$), talc ($Mg_3[Si_4O_{10}(OH)_2]$), serpentine ($(Mg,Fe,Ni)_6Si_4O_{10}(OH)_8$) and amphibole ($Ca_2(Mg,Fe,Al)_5(Al,Si)_8O_{22}(OH)_2$) occur. Furthermore, significant amounts of carbonate minerals such as calcite ($Ca[CO_3]$) and dolomite ($CaMg[CO_3]_2$) are present in some samples. Hey (1999) documented that clay minerals (e.g. smectites) are common in chromitites affected by supergene alteration. All these alteration minerals incorporate certain amounts of water in their structure or, in the case of carbonates, contain considerable amounts of carbon – variables that are not contained in the assay data set. Therefore, low totals are pointing towards

high amounts of alteration minerals but will also change the relative abundance of certain elements within our data set. Due to the relatively high resistance of chromite to alteration the absolute amount of chromite will remain rather consistent, while the overall mineral assemblage can change dramatically and will affect certain elemental ratios. An increase in volume of the seams, for example, will decrease the relative amount of chromite, hence, the Cr_2O_3 concentration decreases. All these parameters can be used as a proxy to detect alteration.

Discussion

In the first part of this section, important findings related to the methodology, the approach of data evaluation and correction – including advantages and limitations – will be discussed. In the second part the mineralogical implications arising from the geochemical changes within the geological architecture will be considered and the clustered geochemical data will be integrated into the spatial – geological – context. Finally, the findings will be critically compared to literature data and implications for mineral beneficiation routes for both, chromite and PGM, in the Bushveld Complex will be deduced.

Methodology

An extensive data set of six major elements and phosphorous was evaluated for a better understanding of the composition of chromitite seams at Thaba mine. Inconsistencies in the data were related to sample batches that were sent to different commercial laboratories during an extended period of time. These inconsistencies were corrected by perturbation of sample batches to a “reference” sample batch, when indicated. Perturbation was only applied where no other possible sources of the differences observed were found, such as systematic differences

due to the area of sampling. Hence, only part of the data set was corrected, as regionally based sampling was widely applied. We showed that a proper sampling strategy as described, e.g. in De Gruijter et al. (2006), is crucial to prevent such inconsistencies or, at least, to allow for better correction methods. Otherwise, a significant, say ~20 %, resampling in the affected areas and re-analysing within one single batch would be necessary to create a data set for levelling the batches to each other. In the case of the Thaba mine, this was not possible due to lack of sampling material remaining in the core repository of the company.

Despite these shortcomings, the applied method of correction produced a consistent data set, at least for further statistical treatment. It should be noted, though, that the correction means that absolute concentrations of certain variables in the corrected data set are not usable anymore, although relative differences are still valid. It also needs to be observed that the totals of the chemical assays are mainly an artefact of the analytical procedure (not reported here). The log-ratio approach as proposed by van den Boogaart and Tolosana-Delgado (2008) was used, to eliminate the resulting biases due to batch and artefact total sum, and to integrate all variables on one scale (P is a trace element on a ppm level).

From chemical clusters to geochemical domains

The chemical composition of the LG-6/LG-6A and MG1/MG2 chromitites at Thaba mine show general trends similar to other locations in the Bushveld Complex. A chemical evolution from rather high Cr_2O_3 concentrations in the LG-6/LG-6A decreasing stratigraphically upwards was shown before (e.g. Naldrett et al. 2009). However, chemical trends in our data set develop gradually, resulting in a distinct separation of LGs and MGs, while separation of LG-6 and LG-6A as well as MG-1 and MG-2 remains difficult and would require a more comprehensive data set.

To reflect the chemical differences between the LGs and the MGs the following cluster analysis was performed separately.

LG chromitites

The integration of geochemical clusters into the geological 3D model allows the recognition of the inherent relations between geochemistry and geological architecture. As shown in Figure 12A and B, clusters form distinct geochemical domains. General trends are similar for both the LG-6 and LG-A. While cluster 1 can be allocated to the southern part of the deposit, clusters 2 and the "supergene" clusters are, in general, located in the north of the mine lease area. Cluster 3 comprises outliers, which form no distinct domain. For the LGs, cluster 1 shows homogeneous elemental distribution including high Cr_2O_3, Al_2O_3 and FeO concentrations, while those of SiO_2 and CaO contents are low. The spatial distribution of this most pristine cluster seems to be connected to troctolite (Figure 12C). Troctolite is believed to cause metasomatization and/or replacement of orthomagmatic mineral assemblages (Voordouw et al. 2010) inducing increasing CaO and Al_2O_3 (plagioclase) and MgO (olivine) concentrations. However, we cannot observe such systematic changes in mineralogy in the majority of samples within cluster 1. Nevertheless, in the rare cases, when troctolites are emplaced in direct contact with the chromitite seams they cause dramatic changes in the chemistry.

Cluster 2 comprises of chromitite samples affected by different types of alteration, with generally lower grades in Cr_2O_3 and increase SiO_2 and/or CaO. According to the alteration markers in Figure 12D these intersections can be assigned to two different sources of alteration. On the one hand, alteration processes associated with the Middellaagte IRUP form a halo of metasomatization/hydrothermal alteration. On the other hand, alteration is related to

serpentinization within and immediately around fault zones in the central portion of the mine lease area.

The “supergene” cluster forms a domain of supergene altered/oxidized ore and displays even lower Cr_2O_3 grades than the pristine and altered domains, while SiO_2, CaO and FeO concentrations increase. As defined above and in accordance to literature (Junge et al. 2015), supergene alteration is restricted to intersections <50 m below surface. It appears reasonable to expect a rapid gradational contact between the supergene and pristine ore zones, although this remains to be tested. This notion is supported by results of the present study, because not all intersections <50 m are classified to the “supergene” cluster. Nevertheless, to define a transition zone between oxidized and pristine ores, the spatial resolution of the data set would have to be significantly higher.

Cluster 3 comprises analyses that can mainly be regarded as outliers. Most of the analyses display high SiO_2, MgO and CaO concentrations. There might be various geological processes responsible for these atypical compositions supergene alteration, strong hydrothermal or metasomatic alteration. That being said, cluster 3 cannot be translated in a distinct geochemical domain but points towards chemical anomalies within the deposit.

MG chromitites

Similar to the LGs, integration into the geological geometry of the defined chemical clusters was performed for the MG chromitites. Due to the limited amount of data for the MG-1 (only ~50 intersections), defining precise domains using chemical clusters was not possible (cf. Figure 10B). Nevertheless, it can be shown that the data sets of MG-1 and MG-2 show a similar

behaviour; it appears thus reasonable to assume that both seams also have similar cluster domains. Furthermore, the interpretation of the clusters in the MGs is virtually identical as for the LGs; hence, cluster 1 is regarded as pristine, cluster 2 is regarded as altered, cluster 3 comprises dominantly outliers and the "supergene" cluster displays supergene altered/oxidized ores. Figure 13A displays the geochemical domains for the MG-2, including a distinct supergene altered domain in the North and a pristine domain in the SW of the mine lease area. Altered samples concentrate around the IRUP in the North-East and along fault structures in the central part of the deposit and overlap with the alteration markers displayed in Figure 13B.

Differences in the visual appearance of the domain structure between LGs and MGs are related to the relative geological position of the LGs and MGs. The MG-2 chromitite is located >100 m higher up in the lithostratigraphy of the Critical Zone of the RLS than the LG-6A. Assuming a dip of the chromitite seams of 30 degrees, a shift of exposure of the chromitites of at least 200 m is expected. If the dip is shallower, the shift will increase even further. Therefore, the oxidized zone of the MGs will be shifted towards the SE. Importantly, a supergene zone cannot be traced to the southern part of the deposit – all data points <50 m below surface fall into the pristine cluster. Obviously, the supergene zone appears not as extensive in the southern part, simply because all the mentioned intersections show a depth between 35 and 50 m.

Summary

Based on a careful evaluation of the assay data base available for four chromitite seams at Thaba Mine, three distinct spatial domains were recognized, which are rather consistent in their extent and distribution between the LGs and MGs. These three spatial domains distinguish rather pristine (least altered orthomagmatic) chromitite (Domain 1) from chromitite that has

been either affected by near supergene (Domain 2) or hydrothermal (Domain 3) alteration. The latter domain includes samples in proximity to faults as well as the IRUP which show signs of alteration. Figure 14A displays a Cr_2O_3-CaO- SiO_2 ternary plot summarizing the main trends of the LG-6 and LG-6A. The LGs all plot alongside a general trend showing an increasing enrichment of Cr_2O_3 with a decrease of their CaO content. The SiO_2 content of the LGs increases from the pristine to supergene domain. Evolution trends of the SiO2 and CaO contents from pristine to altered domains are similar for MGs to the ones seen in LGs (Figure 14B).

Implications for beneficiation of chromite and PGE

Given the fact that the whole rock assays of chromitites can be successfully linked to mineral assemblages within geochemical domains some preliminary conclusions on the probable behaviour during mineral beneficiation for both, chromite and PGE can be drawn. This may be regarded as a preliminary step towards a geometallurgical model, i.e., prediction of processing performance in the resource model (Dunham et al., 2011). According to available literature (e.g. Murthy et al. 2011 and references therein) conventional methods producing chromite concentrates, particularly gravity separation using spirals and wet shaking tables, will cause significant losses of fines to tailings. To avoid these fines an efficient grinding circuit is crucial - and depends largely on a consistent feed quality. At Thaba Mine, the spatial distribution of domains in LG and MG chromitite seams is rather consistent; yet, Cr_2O_3 grades differ significantly between different seams within the same domains. Therefore, it might be challenging to process MGs and LGs together except higher grade ores of the LG seams are blended with lower grade ores of the MG seams.

The feasibility of PGE concentration by flotation will not only depend on grade, but also on mineralogy, mineral association and gangue mineralogy (*e.g.* Penberthy et al. 2000; Chetty et al. 2009, Becker et al. 2013; Ndlovu et al. 2014). Bachmann et al. (2018) showed that alteration of silicate gangue by hydrothermal or supergene processes will also affect PGM and BMS assemblages. Fast-floating PGM closely associated with BMS will be altered to slow-floating PGM associated with chromite and alteration silicates. Alteration will thus, ultimately, result in lower PGE recoveries, as documented by Becker et al. (2014).

Conclusions

This case study illustrates how the combination of geochemical and geological data, complemented by tailored statistical evaluation, can provide a sound foundation for geometallurgical domaining and modelling. According to our assessment, three distinct geochemical domains are developed within the deposit. Firstly, the supergene altered domain is clearly differentiated from domains that are below the extent of modern day weathering. The chromitites below the depth of weathering can be further subdivided into a pristine domain with a predominantly orthomagmatic composition – and a domain affected by hydrothermal alteration processes. The latter domain is developed – sensibly – along fault structures and around the Middellaagte IRUP. These domains are crucial to design a sensible and tailored beneficiation process for chromitite ores, where the pristine domain will show superior processing characteristics for both chromite and PGE beneficiation – as compared to chromitite ores from either the hydrothermal and supergene alteration domains.

The results of this study also strengthen the notion that a proper sampling strategy is crucial to evaluate uncertainties in large chemical data sets. A method to deal with analytical

uncertainties and to minimize their impact on statistical assessments is proposed and successfully applied in this case study. The approach taken in this case study may thus be of general applicability to brownfields exploration and mining projects marred by limited – and inconsistent – geochemical data sets.

Acknowledgements

This is a contribution of the German/South African R&D project AMREP—Applied Mineralogy for Resource Efficiency of Platinum-Group Metals—funded by the German Ministry of Education and Research (BMBF; grant number BMBF 033R119E). We thank the Cronimet Mining Group for providing access to their core shed and drill core intersections from the Thaba mine and for the contribution of additional analytical data as well as information on the local geology and beneficiation. Besides the R software, Mathworks Matlab was used for particular calculations and figures concerning the 3D geometry. Alexander Schwäbe is thanked for his support with the data evaluation for the geological model. The comments of Cynthia Sanchez-Garrido to this manuscript are gratefully acknowledged.

References

Abzalov, M (2008) Quality control of assay data: a review of procedures for measuring and monitoring precision and accuracy. Exploration and Mining Geology, 17(3-4), 131-144.

Aitchison J (1986) The statistical analysis of compositional data. Monographs on Statistics and Applied Probability. Chapman & Hall Ltd., London (UK). (Reprinted in 2003 with additional material by The Blackburn Press). 416p.

Aitchison, J (1990) Relative variation diagrams for describing patterns of compositional variability. Mathematical Geology 22:487–511.

Bachmann K, Osbahr I, Tolosana-Delgado R, Chetty D, Gutzmer J (2018) Variation in platinum group mineral and base metal sulfide assemblages in the Lower Group chromitites of the western Bushveld Complex, South Africa. Can Min, accepted.

[dataset] Bachmann K, Menzel P, Tolosana-Delgado R, Schmidt C, Hill M, Gutzmer J (2018). The use of assay data as a foundation for a geometallurgical model – the case of the Thaba Chromite Mine, South Africa. Journal of Geochemical Exploration, submitted.

Becker M, Yorath G, Ndlovu B, Harris M, Deglon D, Franzidis J-P (2013) A rheological investigation of the behavior of two Southern African platinum ores. Minerals Engineering 49:92–97.

Becker M, Wiese J, Ramonotsi M (2014) Investigation into the mineralogy and flotation performance of oxidised PGM ore. Minerals Engineering 65:24–32.

Chayes F (1960) On correlation between variables of constant sum. Journal of Geophysical Research 65(12):4185–4193.

Chetty D, Gryffenberg L, Lekgetho TB, Molebale IJ (2009) Automated SEM study of PGM distribution across a UG2 flotation concentrate bank: implications for understanding PGM floatability. Journal of the Southern African Institute of Mining and Metallurgy 109(10):587–593

De Gruijter J, Brus DJ, Bierkens MF, Knotters, M (2006) Sampling for natural resource monitoring. Springer Science & Business Media.

De Waal SA, Gauert, CDK (1997) The Basal Gabbro Unit and the identity of the parental magma of the Uitkomst Complex, Badplaas, South Africa. South African Journal of Geology 100:349–361.

Dunham S, Vann J, Coward S (2011) Beyond geometallurgy—gaining competitive advantage by exploiting the broad view of geometallurgy. In Proceedings of the first AusIMM international geometallurgy conference, Brisbane, QLD, Australia, 5–7.

Egozcue JJ, Pawlowsky-Glahn V, Mateu-Figueras G, Barceló-Vidal C (2003) Isometric logratio transformations for compositional data analysis. Mathematical Geosciences 35(3):279–300.

Engelbrecht, JP (1985) The chromites of the Bushveld Complex in the Nietverdiend area. Economic Geology 80(4):896–910.

Evans DM, (2002) Potential for bulk mining of oxidized platinum-group element deposits. Trans Inst Min Metall B 111:81–86.

Evans DM, Buchanan DK, Hall G (1994) Dispersion of platinum, palladium and gold from the main sulphide zone, Great Dyke, Zimbabwe. Trans. Inst. Mining Metall B 103:57–67.

Fourie GP (1959) The chromite deposits in the Rustenburg area. South Africa Geological Survey Bulletin 27:45.

Frenzel M, Hirsch T, Gutzmer J (2016) Gallium, germanium, indium, and other trace and minor elements in sphalerite as a function of deposit type—A meta-analysis. Ore Geology Reviews 76:52–78.

Fahrmeir L, Hammerle A (1984) Multivariate Statistische Verfahren. Walter de Gruijter, Berlin:796p.

Fraley C, Raftery AE (2002) Model-based Clustering, Discriminant Analysis and Density Estimation Journal of the American Statistical Association 97:611–631.

Gence N (1999) Beneficiation of elazig-kefdag chromite by multi-gravity separator, Tr. Journal of Engineering and Environmental Sciences 23:473–475.

Goel RP, (1997) Smelting technologies for ferrochromium production-recent trends. In: Vaish AK, Singh SD, Goswvarni NG, Ramachandrarao P (Editors). Ferro Alloy Industries in the Liberalised Economy. Jamshedpur, 37–50.

Jarvis A, Reuter HI, Nelson A, Guevar E (2008) Hole-filled SRTM for the globe version 4, available from the CGIAR-CSI SRTM 90m Database, http://srtm.csi.cgiar.org.

Junge M, Oberthür T, Kraemer D, Melcher F (2015) Distribution of platinum-group elements in pristine and near-surface ores from the Platreef, northern Bushveld Complex, South Africa. In: André-Mayer AS, Cathelineau M, Muches P, Pirad E, Sindern S (Editors). Mineral Resources in a Sustainable World. 13th Biennial SGA Meeting, 955–958.

Hey PV (1999) The effects of weathering on the UG2 chromitite reef of the Bushveld Complex, with special reference to the platinum-group minerals. South Afr J Geol 102:251–260.

Kinnaird JA, Kruger FJ, Nex PAM, Cawthorn RG (2002) Chromitite formation—a key to understanding processes of platinum enrichment. Applied Earth Science 111(1):23–35.

Koch I (2012) Analysis of multivariate and high-dimensional data theory and practice. Cambridge University Press, Cambridge, UK.

Locmelis M, Melcher F, Oberthuer T (2010) Platinum-group element distribution in the oxidized main sulfide zone, Great Dyke, Zimbabwe. Miner. Deposita 45:93–109.

Maier WD, Barnes S-J, Groves DI (2013) The Bushveld Complex, South Africa: formation of platinum–palladium, chrome- and vanadium-rich layers via hydrodynamic sorting of a mobilized cumulate slurry in a large, relatively slowly cooling, subsiding magma chamber. Mineral Deposita 48:1–56.

Mallet J-L (2002) Geomodelling. Oxford University Press.

Murthy YR, Tripathy SK, Kumar CR (2011) Chrome ore beneficiation challenges & opportunities–a review. Minerals Engineering, 24(5):375–380, DOI: 10.1016/j.mineng.2010.12.001.

Naldrett AJ, Kinnaird J, Wilson A, Yudovskaya M, McQuade S, Chunnett G, Stanley C (2009) Chromite composition and PGE content of Bushveld chromitites: part 1—the lower and middle groups. Trans Inst Min Metall B118:131–161.

Naldrett AJ, Wilson A, Kinnaird J, Yudovskaya M, Chunnett G (2012) The origin of chromites and related PGE mineralization in the Bushveld Complex: new mineralogical and petrological constraints. Mineralium Deposita 47:209–232.

Ndlovu B, Forbes E, Farrokhpay S, Becker M, Bradshaw D, Deglon D (2014) A preliminary rheological classification of phyllosilicate group minerals. Minerals Engineering 55:190–200.

Oberthür T, Weiser TW, Gast L, Kojonen K (2003) Geochemistry and mineralogy of platinum-group elements at Hartley platinum mine, Zimbabwe: Part 2: Supergene redistribution in the oxidized main sulfide zone of the Great Dyke, and alluvial platinum-group minerals. Miner Deposita 38:344–355.

Oberthür T, Melcher F, Buchholz P, Locmelis M (2013) The oxidized ores of the main sulphide zone, Great Dyke, Zimbabwe: turning resources into minable reserves – mineralogy is the key. S. Afr. Inst. Mining Metall. 113:191–201.

Oberthür T, Junge M, Rudashevsky N, de Meyer E, Gutter P (2016) Platinum-group minerals in the LG and MG chromitites of the eastern Bushveld Complex, South Africa. Miner Deposita 51:71–87. DOI: 10.1007/s00126-015-0593-0.

Oppermann L, Junge M, Schuth S, Holtz F, Schwarz-Schampera U, Sauheitl L (2017) Mobility and distribution of palladium and platinum in soils above Lower and Middle Group chromitites of the western Bushveld Complex, South Africa. South Afr J Geol 120(4):511–524, DOI:10.25131/gssajg.120.4.511.

Pearson K (1897) Mathematical contributions to the theory of evolution—on a form of spurious correlation, which may arise when indices are used in the measurement of organs. Proceedings of the Royal Society of London 60(359-367):489–498.

Penberthy CJ, Oosthuyzen EJ, Merkle RKW (2000) The recovery of platinum-group elements from the UG-2 chromitite, Bushveld Complex–a mineralogical perspective. Mineralogy and Petrology 68(1-3): 213–222.

Penberthy CJ, Merkle RKW (1999) Lateral variations in the platinumgroup element content and mineralogy of the UG2 chromitite layer, Bushveld Complex. South African Journal of Geology 102:240–250.

Reid DL, Basson IJ (2002) Iron-rich ultramafic pegmatite replacement bodies within the upper critical zone, Rustenburg layered suite, Northam platinum mine, South Africa. Min Mag 66(6):895–914.

R Core Team (2016) R: A language and environment for statistical computing. R Foundation for Statistical Computing, Vienna, Austria. URL https://www.R-project.org/.

Scoon RN, Mitchell AA (1994) Discordant iron-rich ultramafic pegmatites in the Bushveld Complex and their relationship to iron-rich intercumulus and residual liquids. Journal of Petrology 35(4):881–917.

Scoon RN, Teigler B (1994) Platinum-group element mineralization in the Critical Zone of the Western Bushveld Complex: I. Sulfide-poor chromitites below the UG-2. Economic Geology 89:1094–1121.

Sefako R, Sekgarametso K, Sibanda V (2017) Potential processing routes for recovery of platinum group metals from Southern African oxidized PGM ores: A review. Journal of Sustainable Metallurgy 3(4):797–807.

Smart RSC, Gerson AR, Biesinger MC, Hart, BR (2017) The development of statistical ToF-SIMS applied to minerals recovery by froth flotation. Surface and Interface Analysis 49(13):1387–1396, DOI: 10.1002/sia.6249.

Tolosana-Delgado R, Otero N, Pawlowsky-Glahn V (2005) Some basic concepts of compositional geometry. Mathematical Geology 37(7):673–680.

USGS (2018) Minerals Commodity Summaries, 2018: Chromium. U.S. Geological Survey, U.S. Department of the Interior.

Van den Boogaart KG, Tolosana-Delgado R (2008) "Compositions": a unified R package to analyze compositional data. Computers & Geosciences 34(4):320–338.

Van den Boogaart KG, Tolosana R, Bren M (2014) compositions: Compositional Data Analysis. R package version 1.40-1. https://CRAN.R-project.org/package=compositions.

Viljoen, M (2016) The Bushveld Complex. Episodes 39(2):239–268.

Viljoen MJ, Scoon RN (1985) The distribution and main geologic features of discordant bodies of iron-rich ultramafic pegmatite in the Bushveld Complex. Economic Geology 80(4):1109–1128.

Venables WN, Ripley BD (2002) Modern Applied Statistics with S. Fourth Edition. Springer, New York. ISBN 0-387-95457-0.

von Eynatten H, Tolosana-Delgado R, Karius V, Bachmann K, Caracciolo L (2016) Sediment generation in humid Mediterranean setting: Grain-size and source-rock control on

sediment geochemistry and mineralogy (Sila Massif, Calabria). Sedimentary Geology 336:68–80.

Von Gruenewaldt G (1977) The mineral resources of the Bushveld Complex. Miner Sci Eng 9(2):83–95.

Von Gruenewaldt G, Hatton CJ, Merkle RKW, Gain SB (1986) Platinum-group element–chromite associations in the Bushveld Complex. Economic Geology 81:1067–1079.

Voordouw RJ, Gutzmer J, Beukes, NJ (2010) Zoning of platinum group mineral assemblages in the UG2 chromitite determined through in situ SEM-EDS-based image analysis. Mineralium Deposita 45:147–159. doi: 10.1007/s00126-009-0265-z

Wagner P (1929) The platinum deposits and mines of South Africa. Oliver and Boyd: 338pp.

Zeh A, Ovtcharova M, Wilson AH, Schaltegger U (2015) The Bushveld Complex was emplaced and cooled in less than one million years–results of zirconology, and geotectonic implications. Earth and Planetary Science Letters, 418, 103-114.

Tables

Table 1 Correction of batches in the target seams.

Seam	LG6	LG6A	MG1	MG2
No. of Batches	4	5	3	3
correction of batches	2 into 1	2 into 1	2 into 3	1 into 3

Table 2 Loadings for PCs capturing 90 % variability for PCA of LGs and MGS according to Figure 11.

Loadings			
LGs	**PC1**	**PC2**	**PC3**
Cr_2O_3	-0.46	-0.15	-0.41
FeO	-0.23	b.l.s	-0.19
SiO_2	0.42	0.77	b.l.s
MgO	b.l.s	0.14	b.l.s
Al_2O_3	-0.20	b.l.s	b.l.s
CaO	0.70	-0.59	-0.15
P	-0.14	-0.14	0.88
% var	*61.3*	*83.5*	*94.3*
MGs	**PC1**	**PC2**	**PC3**
Cr_2O_3	-0.35	b.l.s	0.28
FeO	-0.29	b.l.s	0.24
SiO_2	0.27	-0.38	-0.69
MgO	-0.11	-0.24	-0.20
Al_2O_3	-0.27	-0.18	0.21
CaO	0.80	b.l.s	0.47
P	b.l.s	0.87	-0.30
% var	*56.0*	*78.1*	*94.3*

b.l.s – below limit of significance.

Figures

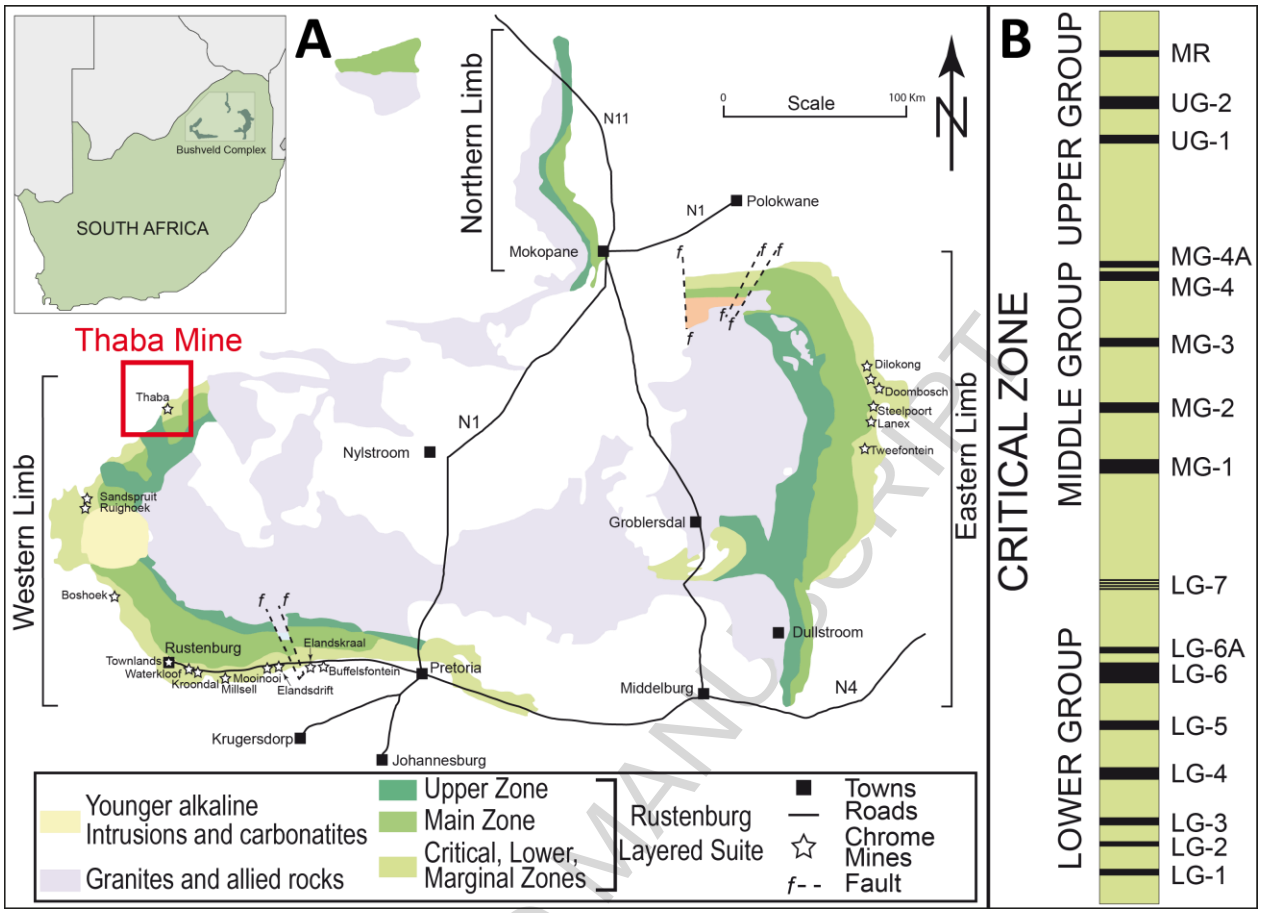

Figure 1 (**A**) Geological Map of the Bushveld Complex. The location of the Thaba mine is marked in red. (**B**) Stratigraphic column of the Critical Zone showing the positions of the major chromitite seams and of the Merensky Reef (MR) (modified from Oberthür et al. 2016).

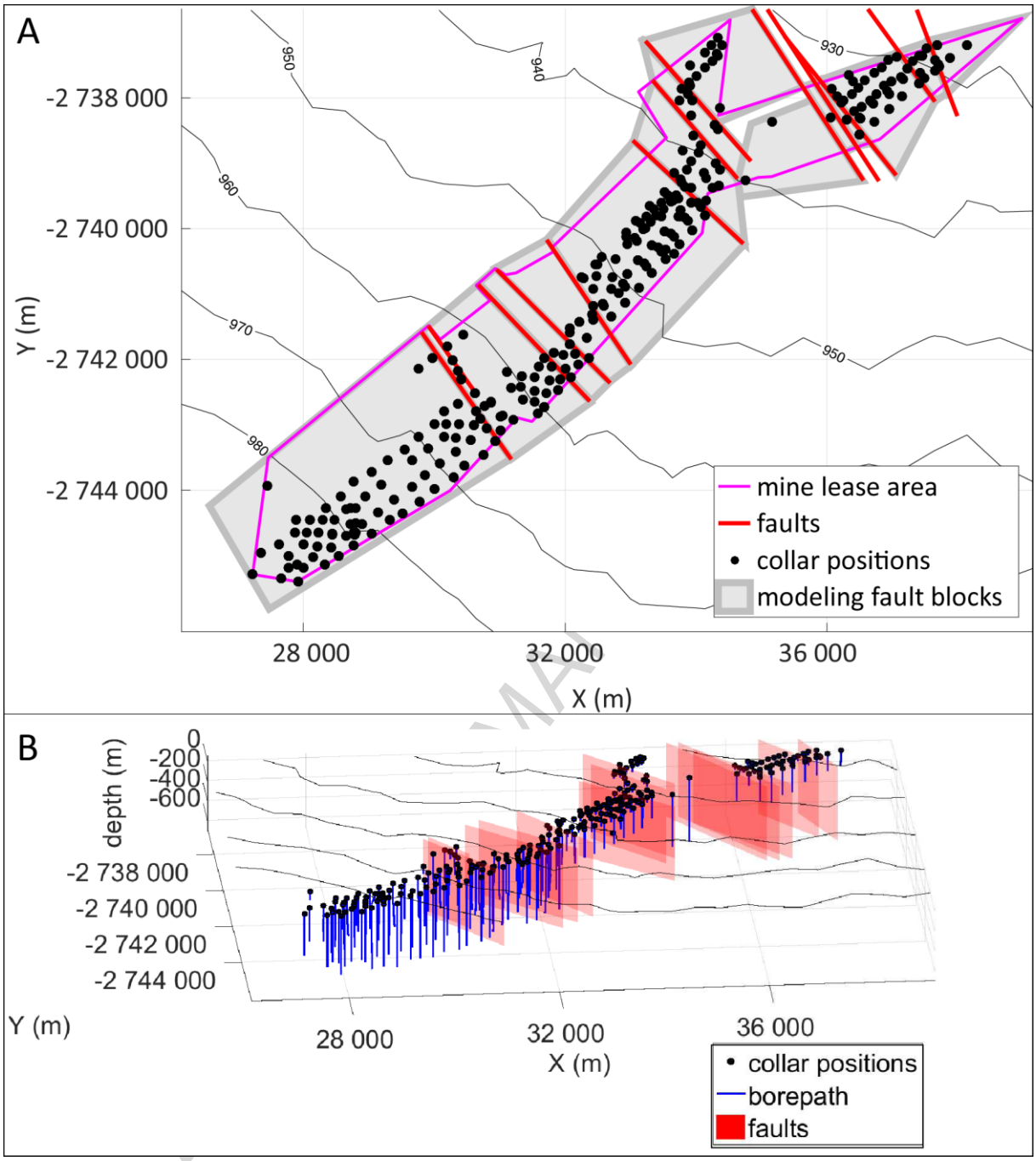

Figure 2 (A) Overview of the data used to create the 3D model. Each borehole (marked by their collar positions as black dots) was assigned to one of 14 fault block (grey polygons) for modelling. The resulting 3D geometries are modelled within these fault blocks. The topography is indicated by black isolines. (B) 3D view of all calculated 3D borepath geometries (blue lines). Based on this calculation, all given lithological depth markers are enhanced with a 3D position based on the associated borehole and stratigraphic unit. A coordinate system called Hartebeesthoek94 / Lo27 (reference meridian 27°, east) was used. The x-coordinate values indicate the distance to the reference meridian (positive direction East). Y-coordinate values

indicate the distance to equator (positive direction North). This applies analogously to all the following figures showing 2D maps and 3D geometries.

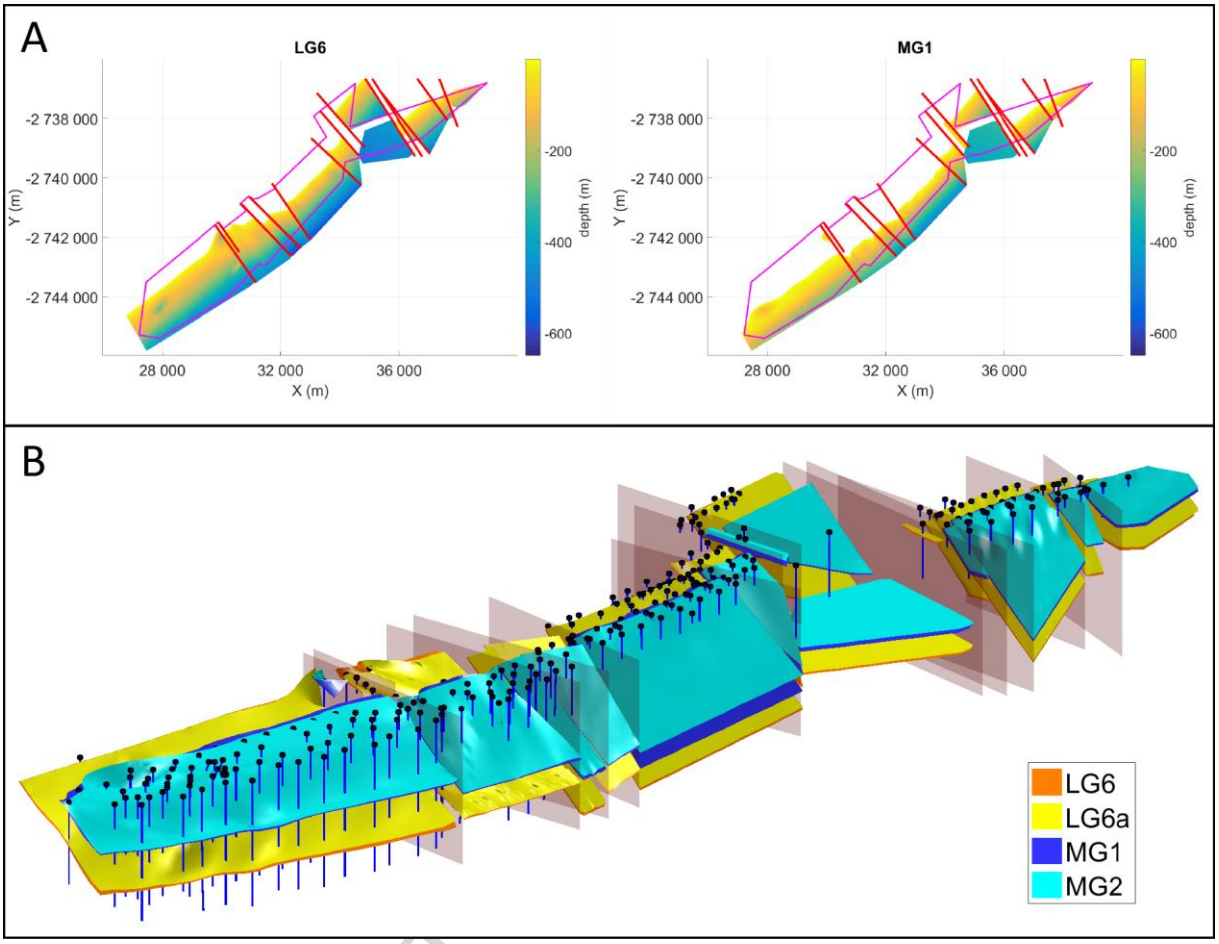

Figure 3 3D model geometry of the Thaba mine. (A) Depth maps for LG6 (left) and MG1 (right). (B) 3D view of the surfaces representing the target seams.

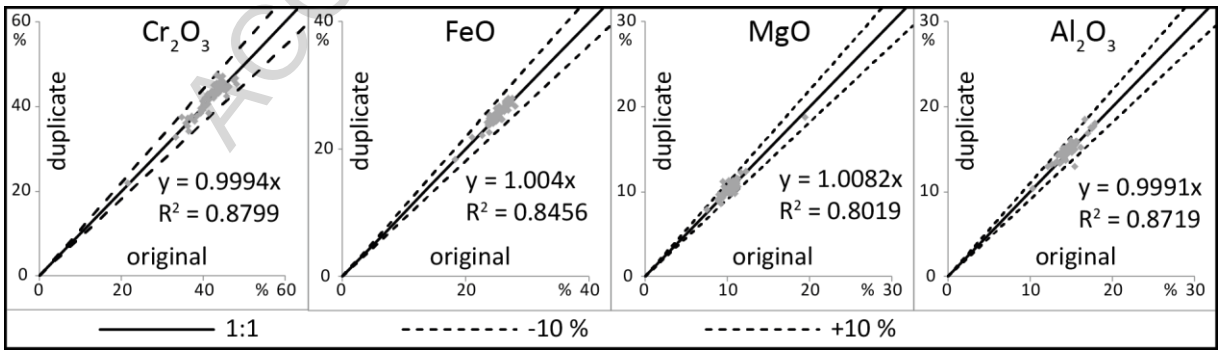

Figure 4 Original versus field duplicate plots for Cr2O3, FeO, MgO and Al2O3 with 10 % relative difference. Formula of the regression line and coefficient of determinations are given in the plots.

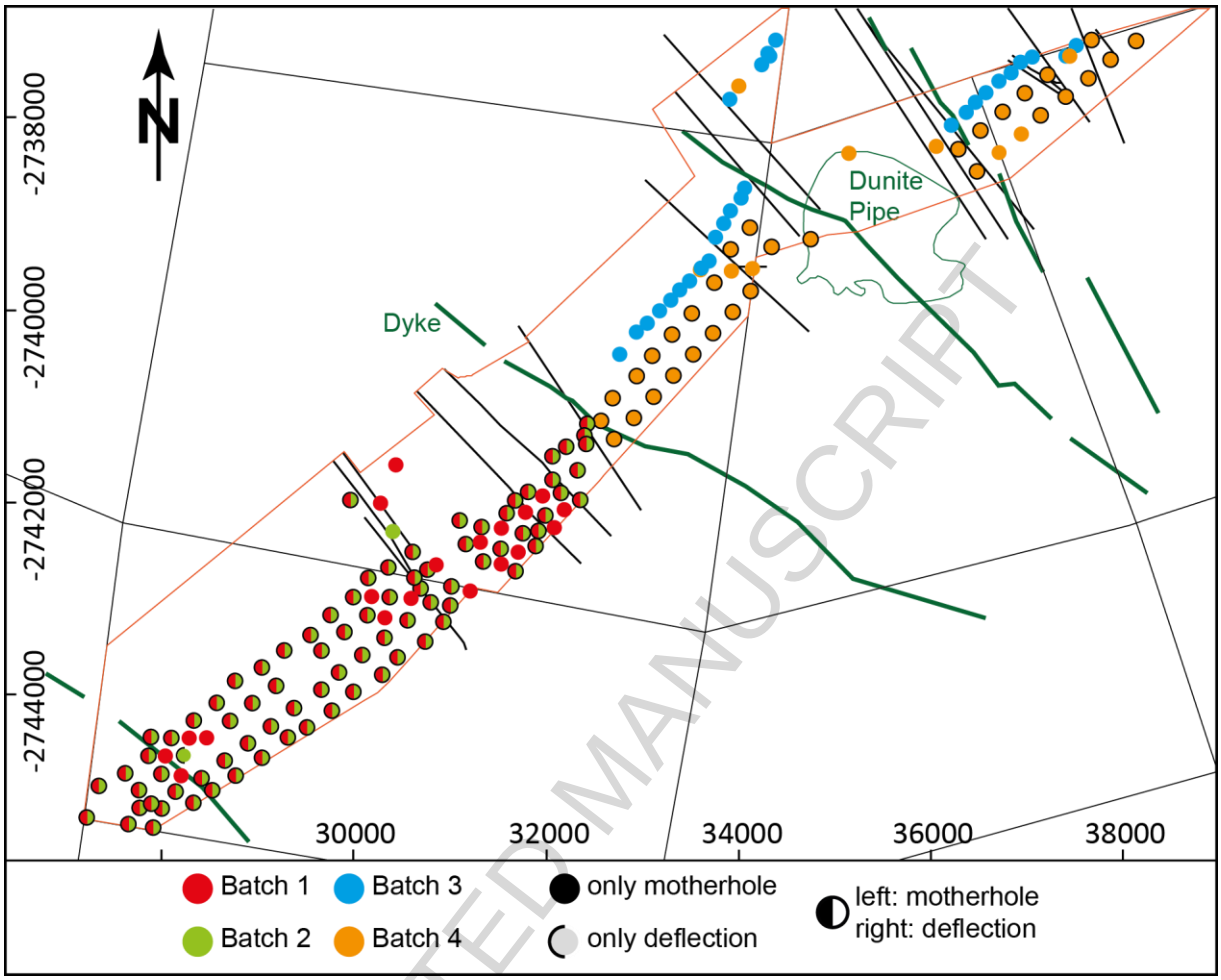

Figure 5 Borehole map of the LG6 in the Thaba mine. Colours show different sampling batches. Please note that batch 1 was analysed by METCHEM Laboratories, while batch 2-4 were sent to Setpoint Laboratories. Batch 4 merges various smaller batches.

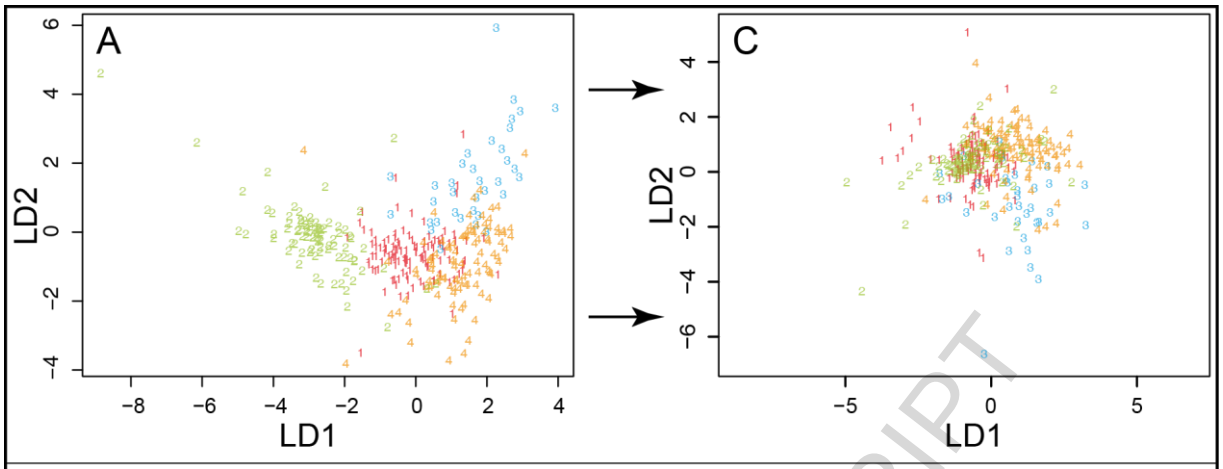

B

Scaling of LD1 and LD2 according to A

	Cr_2O_3	FeO	SiO_2	MgO	Al_2O_3	CaO	P
LD1	-0.45	5.00	0.76	-1.34	-2.06	0.80	-2.71
LD2	-3.22	10.77	-0.26	-3.12	-6.62	0.95	1.50

Figure 6 Results of a batch-wise linear discrimination analysis for the LG6. (A) Plot of LD1 against LD2 based on the uncorrected dataset. (B) Scaling of LD1 and LD2 of the uncorrected dataset. (C) Plot of LD1 against LD2 after the shift of compositional means of batch 2.

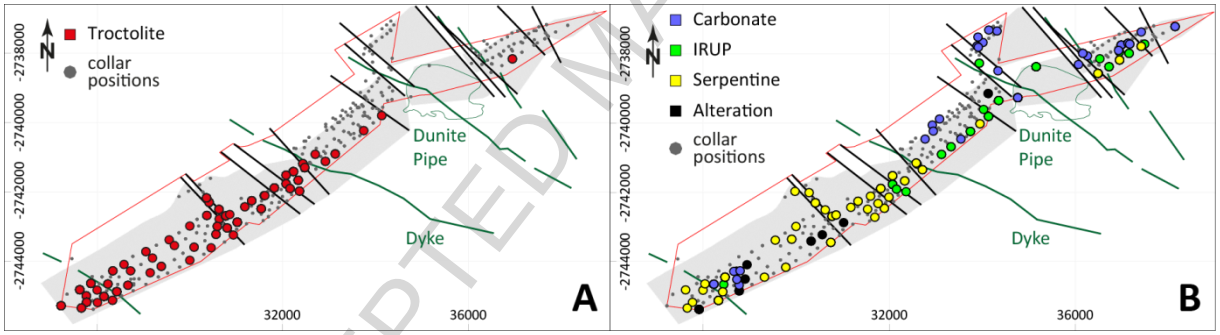

Figure 7 Maps showing the mine lease area and all collar positions. X and Y coordinates are in meter. (A) Map showing all troctolite alteration markers. (B) Map displaying carbonate, IRUP, serpentine and unspecific alteration markers.

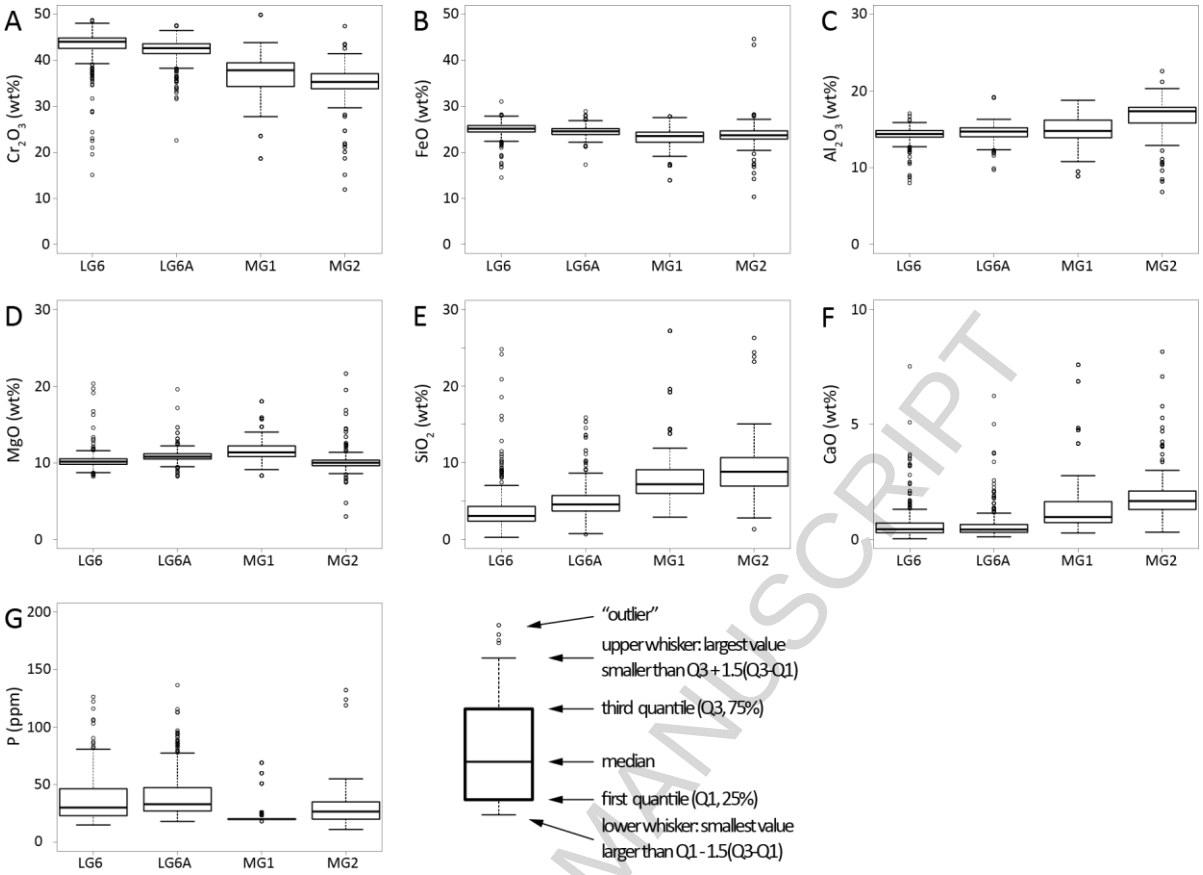

Figure 8 Major element raw data concentrations in oxide wt% (except P – in ppm) for the LG6, LG6A, MG1 and MG2. The variability of individual seams is illustrated in box plots: (A) Cr_2O_3, (B) FeO, (C) Al_2O_3, (D) MgO, (E) SiO_2, (F) CaO, (G) P.

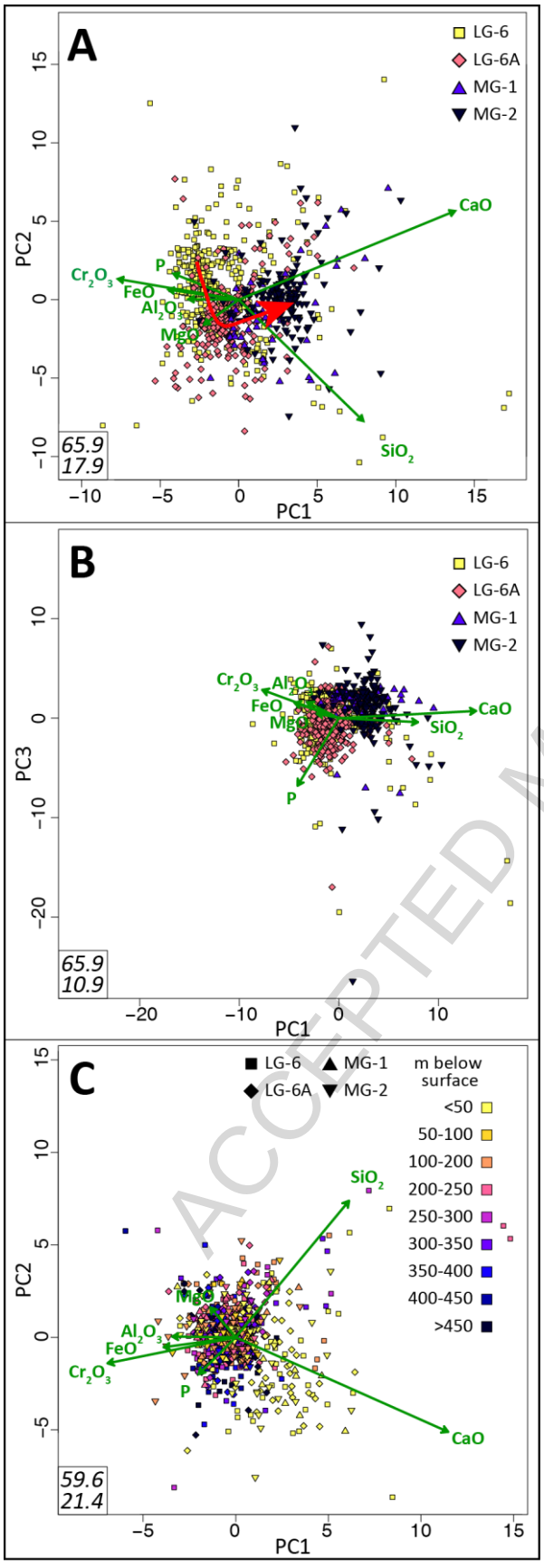

Figure 9 Compositional biplots of major element oxides and phosphorous for the LG-6, LG-6A, MG-1 and MG-2 chromitite seams. (A) shows the first (x-axis) vs. second (y-axis) principal components, (B) shows the first (x-axis) vs. third (y-axis) principal components. Numbers in italics refer to percentages of the total variability explained by PC1 and PC2 (A) or by PC1 and PC3 (B). Similar to (A), (C) displays the first (x-axis) vs. second (y-axis) principal components, however, in (C) the compositional contrast that exists between LG-6 to MG-2 has been minimized by matching the means of each seam.

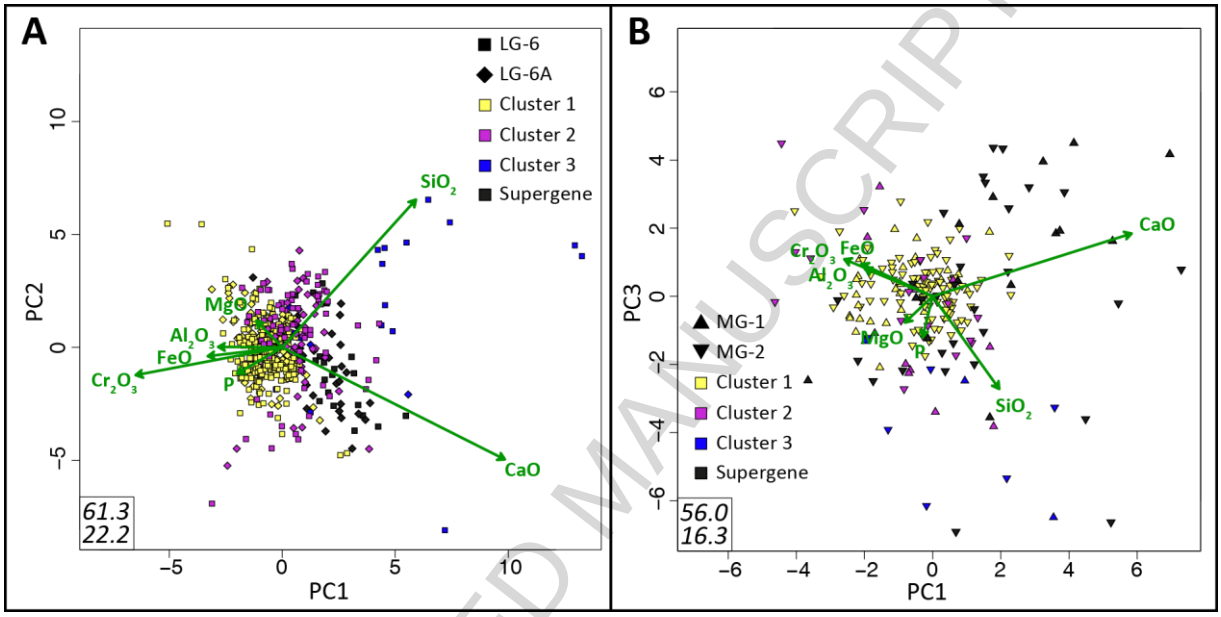

Figure 10 Compositional biplots of major element oxides and phosphorous showing (A) Results of a cluster analysis of LG-6 and LG-6A chromitites (first (x-axis) vs. second (y-axis) principal components) and (B) Results of a cluster analysis of MG-1 and MG-2 chromitites (first (x-axis) vs. third (y-axis) principal components). The compositional contrast that exists between LG-6/ LG-6A and MG-1/ MG-2, respectively, has been minimized by matching the means of each seam.

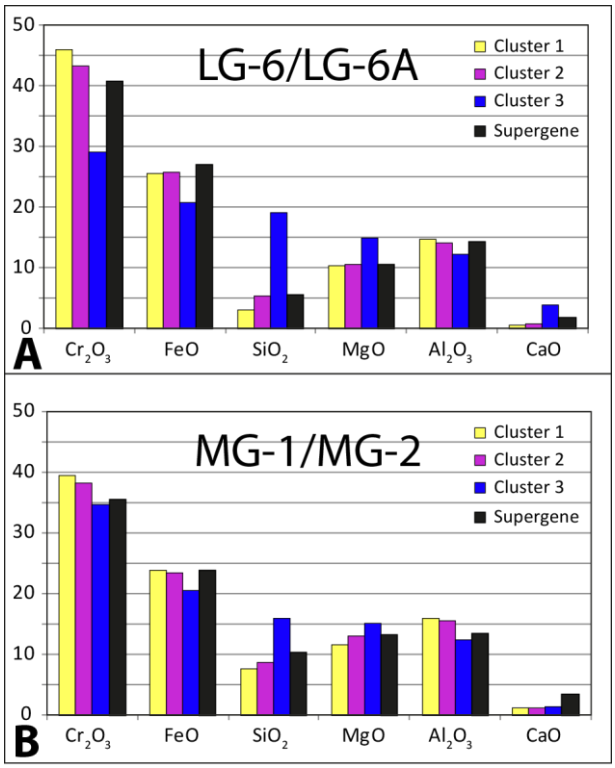

Figure 11 Histograms showing the arithmetical means of cluster determined by PCA. (A) Chemical composition of LG clusters. (B) Chemical composition of MG clusters.

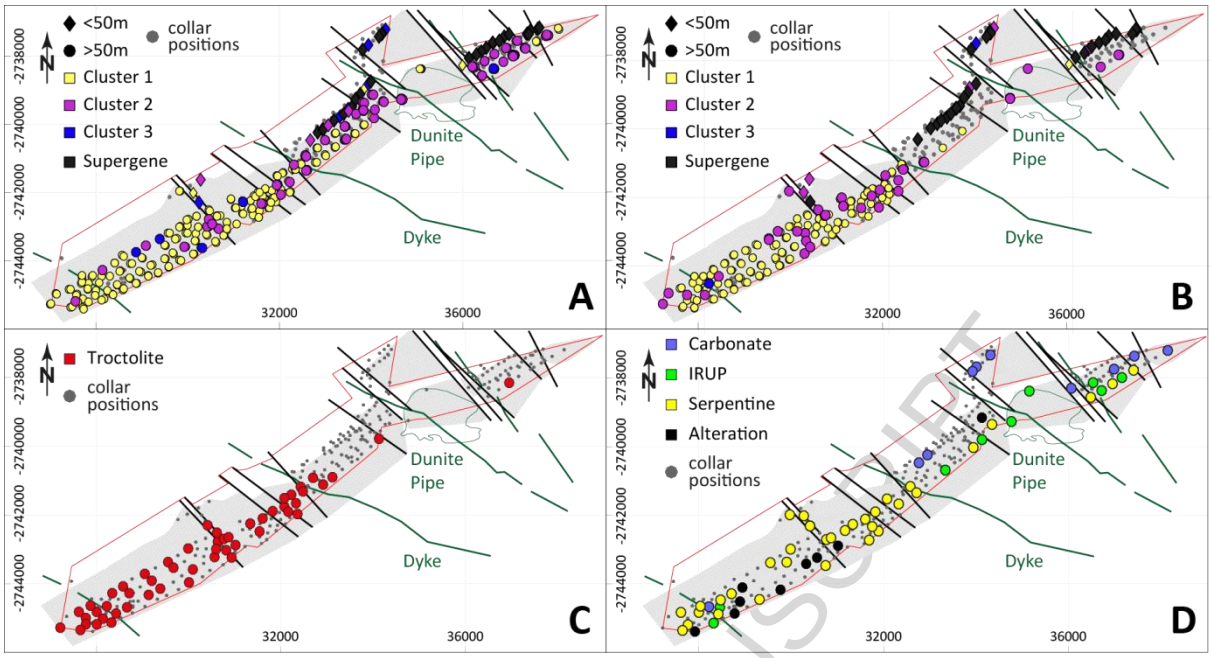

Figure 12 Maps of the mine lease area at the Thaba mine. Maps show all collar positions and the corresponding clustered geochemical data (according to Figure 10) of (**A**) the LG-6 and (**B**) the LG-6A. Maps displaying all alteration markers in close vincinity (150 m vertical and horizontal) to the seam intersections are shown in (**C**) for troctolite and (**D**) for all other alteration markers. Please note, all drill core intersections <50 m depth are displayed as diamonds; drill core intersections >50 m depth are shown as circles. Please further note, the grey shaded areas represent fault blocks. While the northern border of these blocks marks the cross out of the chromitite seam, the southern border is an artefact of modeling.

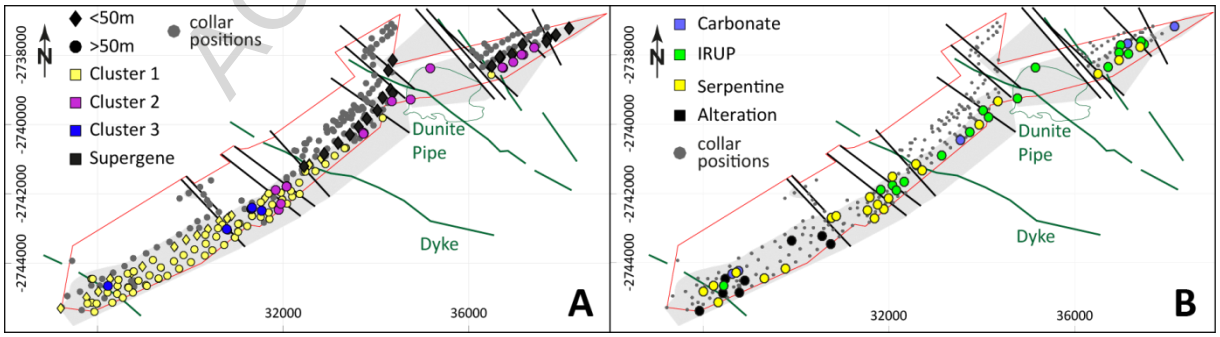

Figure 13 Map of the mine lease area of the Thaba mine. (**A**) Map showing all collar positions and the corresponding clustered geochemical data (according to Figure 11) of the MG-2. (**B**) Map displaying all alteration markers in close vincinity (150 m vertical and horizontal) to the

MG-2 seam intersections for all alteration markers except troctolite. Please note, all drill core intersections <50 m depth are displayed as diamond; drill core intersections >50 m depth are shown as circles. Please further note, the grey shaded areas, representing fault blocks. While the northern border ofthese blocks marks the cross out of the chromitite seam, the southern border is an artefact of modeling.

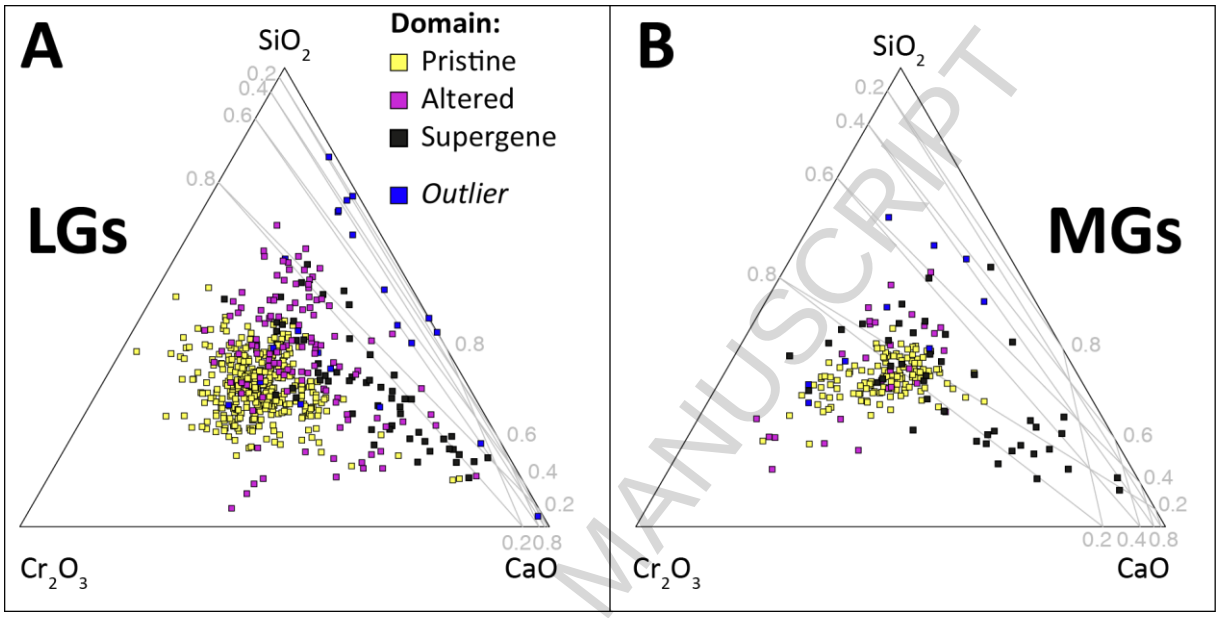

Figure 14 Ternary diagrams for Cr_2O_3 – CaO – SiO_2 centered for their geometrical mean. Data is displayed for three interpreted domains and the cluster *outlier* for (**A**) LGs and (**B**) MGs.

Highlights

- Geological and geochemical modelling based on a large dataset
- Sound geochemical interpretation of four economically important chromitite seams
- Development of geochemical domains is aided by principal component and cluster analysis
- Maximizing the outcome of legacy databases by dealing with possible inconsistencies
- Improving of minerals beneficiation by understanding of geological features